Received May 23, 2021, accepted July 20, 2021, date of publication July 26, 2021, date of current version August 23, 2021.
Digital Object Identifier 10.1109/ACCESS.2021.3100084

Phase Current Reconstruction With Dual-Sensor for Switched Reluctance Motor Drive System

HE CHENG, (Member, IEEE), SHUAI MI, ZELU WANG, DALI SHAO, HAONAN WU, WENJU YAN, (Member, IEEE), AND DONGSHENG YU, (Member, IEEE)
School of Electrical and Power Engineering, China University of Mining and Technology, Xuzhou 221116, China
Corresponding author: He Cheng (chenghecumt@163.com)

This work was supported by the Fundamental Research Funds for the Central Universities under Grant 2018QNA07.

ABSTRACT Due to the rugged construction, high starting torque, wide speed range, inherent fault-tolerance and high operating efficiency, switched reluctance motors (SRMs) have been used in many fields such as household appliances, electric vehicles and industrial drives. At low and medium speeds, the current chopping control (CCC) are usually used for SRMs. The current sensors must be connected in series with each phase winding for detecting the phase current, and the number of sensors is usually equal to the number of motor phases. In order to reduce the number of current sensors and the cost of the drive system, this paper propose a general phase current reconstruction method for SRM drive system with two current sensors. Firstly, the excitation, freewheeling and demagnetization circuits of the asymmetric half-bridge power converter are separated into two different paths. The sensors placement method, winding connection method and calculation formula of each phase current are introduced in detail. Then the influence of the turn-off angles on the overlap interval of each phase current is analyzed, and the proposed reconstruction method is further extended to multi-phase SRM. This method can simplify the current decoupling process and is easy to implement without changing the asymmetric half-bridge topology and operating states. Finally, the feasibility of the proposed phase current reconstruction algorithm is verified by simulation and experiment.

INDEX TERMS Switched reluctance motor, phase current reconstruction, two current sensors.

I. INTRODUCTION

Switched Reluctance Motor (SRM) has the advantages of rugged construction, low cost high starting torque, wide speed range and inherent fault-tolerance [1]–[3], which have been used in many fields such as household appliances, electric vehicles and industrial drives [4]–[8]. The current chopping control (CCC) method for speed regulation in the low speed range are usually adopted, and the current value of each phase winding must be obtained [9], so the current sensor must be employed in each phase [10]. Usually, the number of current sensors depends on the number of phases. At present, the application of multi-phase SRMs for reducing torque ripple is gradually increasing. This also means that the traditional method of current sampling will use a large number of current sensors, which undoubtedly increases the system volume and cost [4], [11]–[15]. Therefore, the exploration of the reconstruction method of each phase current with fewer sensors has become one of the hot research directions [16].

Three optimization schemes for different positions of sensors are discussed in [17] to reduce the number of sensors, and then the advantages and disadvantages of various schemes under different placement methods and different numbers of sensors are analyzed. A universal two-sensor current detection scheme for multiphase SRM control with multiphase excitation, by selecting the currents flowing through each sensor is proposed in [18]. This method is applicable for all three-phase, four-phase, five-phase, and six-phase drives, without external circuits and any changes in converter topologies. A novel phase current reconstruction method from the dc-link current employing double high-frequency pulses injection is proposed in [19]. In the method, the double high-frequency pulses with phase shift and large duty cycles are injected to the down switches in the two-phase excitation region, and two A/D converters are triggered, respectively, in the PWM pause middle to sample the dc-link current,

The associate editor coordinating the review of this manuscript and approving it for publication was Christopher H. T. Lee.

and all phase currents in the phase excitation regions are effectively reconstructed by combining with the turn-on and turn-off information. The proposed method can realize the synchronization between the high-frequency pulses and the A/D samplings to obtain high-quality reconstructed phase currents. In [20], an improved converter topology is proposed, which has fewer electronic components and a more compact structure compared with the conventional asymmetrical half-bridge converter. By adopting the improved converter, the cost and volume of the drive system are both reduced with the less electronic components. Then, an advanced pulse injection technology is developed to obtain the phase currents. The proposed method proposes a promising solution to the voltage penalty problem caused by the other existing strategies, which significantly increases the sampling accuracy without the restriction of the duty cycle of injected pulse. Literature [21] proposes a promising cost-effective phase current detection scheme for different multiphase switched reluctance motors (SRMs) by employing the multiplexed current sensors. The number of sensors is $m/2$ for the odd-numbered multiphase SRM with m phases, and the number of sensors is $(n + 1)/2$ for the even-numbered multiphase SRM with n phases. By building the matrix functions to express the relationship between phase currents and sensor currents, the phase currents can be calculated in real time with a simple algorithm and fewer current sensors. The method has high universality and can achieve the intact phase current detection without losing any excitation, freewheeling, and demagnetization currents. Moreover, the presented method is easy to implement without any converter change and pulse injection, which shows great potential for massive industrial application to avoid the voltage penalty, current distortion, higher switching loss, and further electromagnetic interference issues.

In the existing literatures, one or two current sensors are used to reconstruct the phase current. The methods with one current sensor require high-frequency pulse injection to the non-conducting phase and decouple the currents of each phase according to the rotor position information. Although this method requires the least number of sensors, it will increase the sampling complexity, and the injected pulses will also affect the sampling accuracy. The methods with two current sensors can avoid the complicated pulse injection process. The phase current decoupling can be completed by solving some simple equations according to the rotor position information. Based on the previous studies, this paper proposes a universal phase current reconstruction method with two current sensors. The effectiveness and reliability of the proposed method are verified through theoretical analysis, formula derivation, simulation, and experiment.

II. TRADITIONAL CURRENT SAMPLING METHOD

Figure 1 shows the asymmetric half-bridge converter structure and the placement position method of the current sensors in the traditional sampling mode for a three-phase SRM drive system. Each phase consists of two switches and

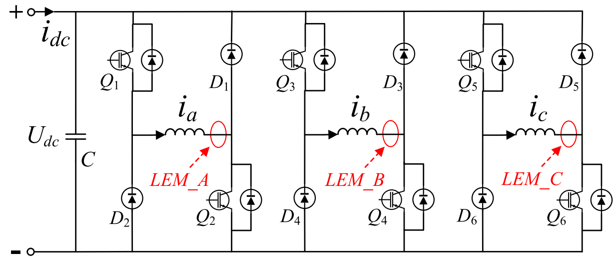

FIGURE 1. Sensor placement position under the traditional current sampling method.

two freewheeling diodes, and can be excited independently. Q_1, Q_3, and Q_5 are the upper tubes of each phase. The upper tubes control signals of each phase are determined by the current chopping signals and the rotor position signals. Q_2, Q_4, and Q_6 are down tubes, which are only determined by the position signals of each phase. D_1, D_2 to D_5, D_6 are the freewheeling diodes, which return the energy stored in the windings back to the power supply during the demagnetization stage. i_a, i_b, and i_c are three-phase winding currents, and *LEM_A*, *LEM_B*, and *LEM_C* are current sensors placed on the three-phase windings. It can be seen that the current sensors are in series with phase windings, and the number of sensors is equal to the number of motor phases.

The rotor period of the three-phase 12/8 structure SRM is 45°. The inductance of each phase is symmetry and the maximum conduction angle (the maximum excitation angle) is usually half of the rotor period value, which is 22.5°. The adjacent phase is staggered by 15°, and the specific calculation formula is as follows:

$$C_e = \frac{360^\circ}{N_r} \tag{1}$$

$$\theta_{\max} = \frac{C_e}{2} \tag{2}$$

$$\theta_s = \frac{C_e}{m} \tag{3}$$

where C_e represents the rotor period, N_r represents the number of rotor poles, $\theta_{\max}$ is the maximum excitation angle, and θ_s is the lagging angle of each phase.

From the basic structure and parameters of the selected motor, the following diagram of the corresponding relationship between phase current and inductance can be obtained. The current waveform is different depending on the selection of the turn-on and turn-off angles. The position near the minimum inductance is 0 which can be regarded as the turn-on angle, and the position near the maximum inductance is 22.5° which can be regarded as the turn-off angle.

Figure 2 (a) shows the three-phase inductance waveforms under unsaturated conditions. According to the dotted line shown in the figure above, the entire inductance cycle during one rotor period is divided into six intervals. Take phase A for example, internals I, II, and III are three inductance rising sub-regions of phase A, respectively. In interval I, the inductances of phase A and phase C both are monotonic increase. In interval II, only the phase A inductance

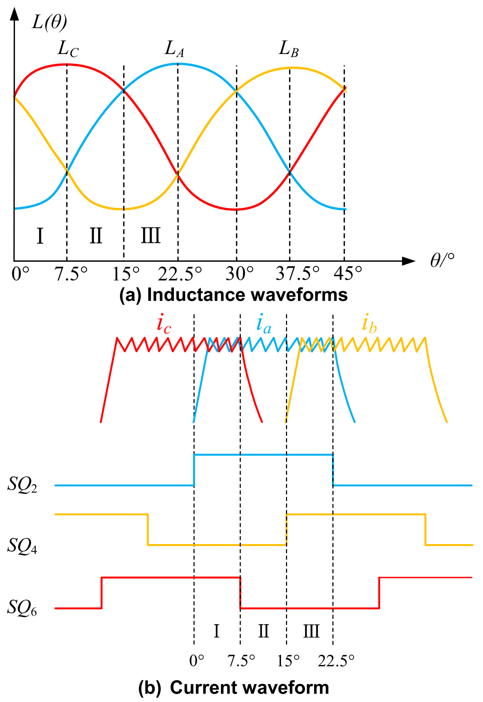

FIGURE 2. Inductance and current characteristic diagram for three-phase motor.

is rising. In interval III, both phases A and B inductance are rising.

SQ_2, SQ_4, and SQ_6 in Figure 2(b) respectively represent the control signals of three-phase down tubes. Also take phase A as an example, the start time of high-level corresponds to the 0° rotor position for turn-on angle, and the end time of high-level corresponds to 22.5° rotor position for turn-off angle. The high-level width includes all the inductance rising intervals of phase A in Figure 2(a), and phases B and C lag behind phase A by 15° and 30° successively. It can be seen from the current waveform in the above figure that there exists simultaneous conduction section of the two phases at the same time. If the current of each phase is not overlapped, a single current sensor can be used to obtain the current without any decoupling process. Therefore, the phase current reconstruction methods proposed in this paper are based on the premise that the two phases currents have overlapping regions.

From the above analysis, it can be seen that there are overlapped and non-overlapped conduction internals between two phases during the conduction angle for three-phase SRM, and the width of the overlap zone is determined by the turn-on and turn-off angles. Therefore, the current of each phase can be decoupled according to the position signal and reasonable sensor placement.

III. TWO-SENSOR PHASE CURRENT RECONSTRUCTION METHOD

This paper proposes a universal two-sensor phase current reconstruction method for SRM. Take a three-phase SRM

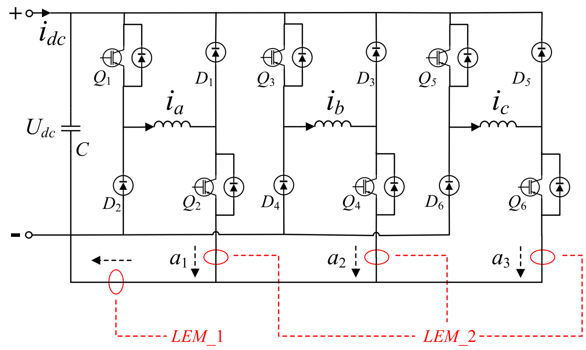

FIGURE 3. Schematic diagram of two sensors placement.

for instance, the modified asymmetric half-bridge power converter topology and placement position of two current sensors are shown in Figure 3. The emitters of down tubes in each phase are connected to the negative pole of the power supply to form a new circuit which contains only the excitation and freewheeling paths. The demagnetization path is still formed by the antiparallel diodes of up and down switches in each phase. The current sensor *LEM_1* is placed near the negative pole of the power supply. The emitters of the down tubes of three phases all pass through the sensor *LEM_2*. i_a, i_b, and i_c are the winding currents of each phase, and the current coefficients a_1, a_2, and a_3 indicate the number of passing through the *LEM_2*. The arrow direction in figure is the positive direction of the current, that is, the coefficient value is positive when the current is in the positive direction, and the coefficient value is negative when the current is in the opposite direction.

According to the above dual current sensors placement method, the following formula can be obtained:

$$i_{L1} = i_a + i_b + i_c \tag{4}$$

$$i_{L2} = a_1 i_a + a_2 i_b + a_3 i_c \tag{5}$$

where i_{L1} and i_{L2} represent the sampling current values of current sensors *LEM*_1 and *LEM*_2 respectively. The i_{L1} is the sum of the winding currents of each phase, that is, the coefficient of each phase in the above (4) is 1. The value of i_{L2} is determined by the current coefficient which can be set as required in each phase. Because two phase windings can be conducted at most at the same time, the currents of each phase can be obtained in the conduction interval by solving equations (4) and (5) according to the rotor position information of each phase. The solution method will be introduced below.

A. ANALYSIS OF PHASE CURRENT RECONSTRUCTION METHOD

For a three-phase 12/8 SRM, it can be seen from Figure 2 that there are two cases of one-phase conduction and two-phase conduction in this area. During the demagnetization stage, the phase current flows back to the power supply through the freewheeling diodes, and the phase current is zero during this stage by using the proposed detection method. In the inductance rising area of phase A, the current coefficients a_1, a_2, and a_3 are set as 2, 1, and -1, respectively. When the rotor is in the interval I, there exist currents in phases A and C, and the phase B current is zero. The following formula can be obtained:

$$i_{L1} = i_a + i_c \tag{6}$$
$$i_{L2} = 2i_a - i_c \tag{7}$$

In interval II, only phase A has current, and the currents in phases B and C both are zero. This moment:

$$2i_{L1} = i_{L2} = 2i_a \tag{8}$$

In interval III, there exist currents in phases A and B, and the phase C current is zero. The formula can be obtained:

$$i_{L1} = i_a + i_b \tag{9}$$
$$i_{L2} = 2i_a + i_b \tag{10}$$

When the control signals of the down tubes are high level in Figure 2, SQm is set as 1(m = 2, 4 or 6), otherwise SQm is set as 0. Then in interval I, $SQ2 = 1$, $SQ4 = 0$ and $SQ6 = 1$. In interval II, $SQ2 = 1$, $SQ4 = 0$ and $SQ6 = 0$. In interval III, $SQ2 = 1$, $SQ4 = 1$, $SQ6 = 0$. Based on the above formula and rotor position signals, the sampling values of current sensors *LEM_1* and *LEM_2* during a complete rotor period can be obtained, as shown in Table 1 below.

TABLE 1. Sampling values of two current sensors under different position signals.

$SQ2$	$SQ4$	$SQ6$	i_{L1}	i_{L2}
1	0	1	i_a+i_c	2i_a-i_c
1	0	0	i_a	2i_a
1	1	0	i_a+i_b	2i_a+i_b
0	1	0	i_b	i_b
0	1	1	i_b+i_c	i_b-i_c
0	0	1	i_c	-i_c

It can be seen from Table 1 that when the position signals SQm of the lower tube of each phase is 1, the corresponding phase current would exist. When the position signal is 0, the corresponding phase current value is zero. In the current overlapping area, the sampling values of the two sensors are the sum or difference between the present phase current and the adjacent phase current. Since i_{L1} and i_{L2} are known quantities, the current of each phase can be obtained by solving the binary linear equations according to the rotor position information. The specific solution formula for phase A current is given below:

$$i_a = \begin{cases} (i_{L1} + i_{L2})/3 & SQ2 = 1,\ SQ4 = 0,\ SQ6 = 1 \\ i_{L1} = i_{L2}/2 & SQ2 = 1,\ SQ4 = 0,\ SQ6 = 0 \\ i_{L2} - i_{L1} & SQ2 = 1,\ SQ4 = 1,\ SQ6 = 0 \end{cases} \tag{11}$$

The calculation formula for phase B current is:

$$i_b = \begin{cases} 2i_{L1} - i_{L2} & SQ2 = 1,\ SQ4 = 1,\ SQ6 = 0 \\ i_{L1} = i_{L2} & SQ2 = 0,\ SQ4 = 1,\ SQ6 = 0 \\ (i_{L1} + i_{L2})/2 & SQ2 = 0,\ SQ4 = 1,\ SQ6 = 1 \end{cases} \tag{12}$$

The calculation formula for phase C current is:

$$i_c = \begin{cases} (2i_{L1} - i_{L2})/3 & SQ2{=}1,\ SQ4{=}0,\ SQ6{=}1 \\ (i_{L1} - i_{L2})/2 & SQ2{=}0,\ SQ4{=}1,\ SQ6{=}1 \\ i_{L1}{=}(-i_{L2}) & SQ2{=}0,\ SQ4{=}0,\ SQ6{=}1 \end{cases} \tag{13}$$

B. EXTENSION OF PHASE CURRENT RECONSTRUCTION METHOD

For a four-phase SRM, such as the 8/6 structure, according to (1) to (3), it can be seen that the rotor period is 60°, and the maximum conduction angle is 30°, and each phase is staggered by 15°. The phases A and C cannot be conducted simultaneously, as well as for phases B and D. It also can be seen that in the current overlapping region, at most two-phase windings can be conducted at same time. So, the dual-sensor reconstruction method mentioned above can also can be applied. When the turn-on and turn-off angles are set at 0° and 30° respectively, the four-phase current waveforms and the corresponding control signals of down switches are shown in the figure 4.

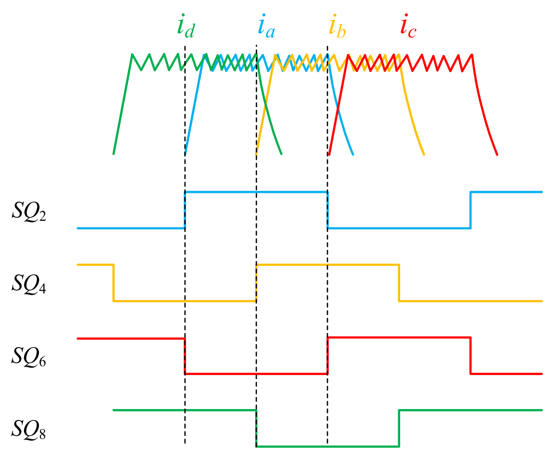

FIGURE 4. Corresponding diagram of four-phase current and position signal under the turn-on angle of 0° and the turn-off angle of 30°.

Take phase A for instance, it can be seen from the figure above that the conduction interval of phase A can be divided into two parts as shown by the dotted line, which are the overlapping area of phases A and D, and the overlapping area of phases A and B, respectively. In the whole conduction internal, the phase currents are overlapping. Compared with a three-phase SRM, there are no current non-overlapping area when the turn-on and turn-off angles are set at 0° and 30° for four-phase SRM. The phase current reconstruction method proposed for the three-phase SRM also can be used to obtain the phase current of phases A, B, C and D in each conduction sub-interval. The current sensors placement method is the same as that shown in Figure 3. The current coefficients of each phase are represented by a1, a2, a3, and a4. The current reconstruction calculation formula is as follows:

$$i_a=\begin{cases}(a_4\cdot i_{L1}-i_{L2})/(a_4-a_1) & SQ2=1,\ SQ4=0,\ SQ6=0,\ SQ8=1\\(a_2\cdot i_{L1}-i_{L2})/(a_2-a_1) & SQ2=1,\ SQ4=1,\ SQ6=0,\ SQ8=0\end{cases}\tag{14}$$

$$i_b=\begin{cases}(a_1\cdot i_{L1}-i_{L2})/(a_1-a_2) & SQ2=1,\ SQ4=1,\ SQ6=0,\ SQ8=0\\(a_3\cdot i_{L1}-i_{L2})/(a_3-a_2) & SQ2=0,\ SQ4=1,\ SQ6=1,\ SQ8=0\end{cases}\tag{15}$$

$$i_c=\begin{cases}(a_2\cdot i_{L1}-i_{L2})/(a_2-a_3) & SQ2=0,\ SQ4=1,\ SQ6=1,\ SQ8=0\\(a_4\cdot i_{L1}-i_{L2})/(a_4-a_3) & SQ2=0,\ SQ4=0,\ SQ6=1,\ SQ8=1\end{cases}\tag{16}$$

$$i_d=\begin{cases}(a_3\cdot i_{L1}-i_{L2})/(a_3-a_4) & SQ2=0,\ SQ4=0,\ SQ6=1,\ SQ8=1\\(a_1\cdot i_{L1}-i_{L2})/(a_1-a_4) & SQ2=1,\ SQ4=0,\ SQ6=0,\ SQ8=1\end{cases}\tag{17}$$

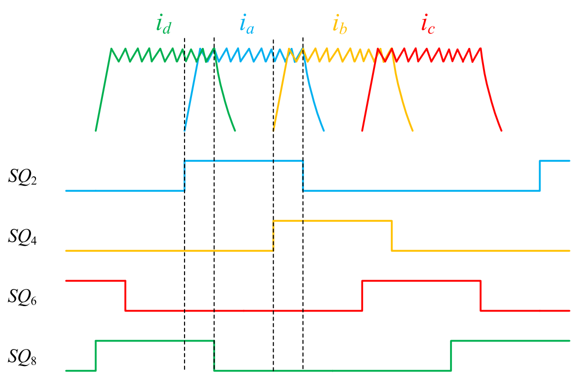

FIGURE 5. Corresponding diagram of four-phase current and position signal under the turn-on angle of 0° and the turn-off angle of 20°.

When the turn-off angle is decreased, the conduction interval would be reduced and the current overlapping area of each phase will also be reduced accordingly. For the four-phase SRM, there will exist both current overlapping and non-overlapping areas in the whole conduction interval. And the three sub-intervals described above are presented in Figure 5. In this condition, the current reconstruction formulas of each phase for the four-phase SRM are similar to those for the three-phase SRM, which are not given again.

For a multi-phase SRM, the number of current overlapping phases can also be reduced to two phases by adjusting the turn-on and turn-off angles appropriately. At this point, the current reconstruction method proposed above also can be used. For example, for an N-phase SRM, the current reconstruction calculation formulas for the first and last two phases windings are:

$$i_a=\begin{cases}(a_n i_{L1}-i_{L2})/(a_n-a_1) & SQ2=1,\ SQ4=0,\ \cdots,\ SQ2N=1\\ i_{L1}=i_{L2}/a_1 & SQ2=1,\ SQ4=0,\ \cdots,\ SQ2N=0\\(a_2 i_{L1}-i_{L2})/(a_2-a_1) & SQ2=1,\ SQ4=1,\ \cdots,\ SQ2N=0\end{cases}\tag{18}$$

$$i_n=\begin{cases}(a_{n-1} i_{L1}-i_{L2})/(a_{n-1}-a_n) & SQ2=0,\cdots,SQ(2N-2)=1,\ SQ2N=1\\ i_{L1}=i_{L2}/a_n & SQ2=0,\cdots,SQ(2N-2)=0,\ SQ2N=1\\(a_1 i_{L1}-i_{L2})/(a_1-a_n) & SQ2=1,\cdots,SQ(2N-2)=0,\ SQ2N=1\end{cases}\tag{19}$$

where a_1, a_2, a_{n-1}, and a_n represent the current coefficients of the first phase, the second phase, the N-1th phase and the Nth phase, respectively, *SQ*(*2N-2*) and *SQ2N* represent the control signals of down switches for N-1th and Nth phase respectively. In view of the above analysis, the reconstruction formulas of any phase current of N-phase motor can be expressed as:

$$i_k=\begin{cases}(a_{k-1} i_{L1}-i_{L2})/(a_{k-1}-a_k) & \cdots,SQ(2k-2)=1,\ SQ2k=1,\ SQ(2k+2)=0,\cdots\\ i_{L1}=i_{L2}/a_k & \cdots,SQ(2k-2)=0,\ SQ2k=1,\ SQ(2k+2)=0,\cdots\\(a_{k+1} i_{L1}-i_{L2})/(a_{k+1}-a_k) & \cdots,SQ(2k-2)=0,\ SQ2k=1,\ SQ(2k+2)=1,\cdots\end{cases}\tag{20}$$

where a_k, a_{k-1} and a_{k+1} (k = 2, 3, ..., N-1) represent the current coefficients of the (K-1)th, Kth and (K + 1)th phases respectively. *SQ(2K-2)*, *SQ(2K)* and *SQ(2K + 2)* represent the control signals of down switches for the (K-1)th, Kth and (K + 1)th phase, respectively.

IV. SIMULATION AND EXPERIMENTAL VERIFICATION

In order to verify the feasibility of the phase current reconstruction method proposed in this paper, a three-phase 12/8 SRM is used to verify the above algorithm. The motor parameters are shown in Table 2. The experimental platform

TABLE 2. Motor parameters.

Parameter	Rated value
Motor phase number	3
Stator and rotor stages	12/8
Overload multiple	2~4
Rated power	1.5kW
Rated voltage	36V
Rated speed	3000r/min

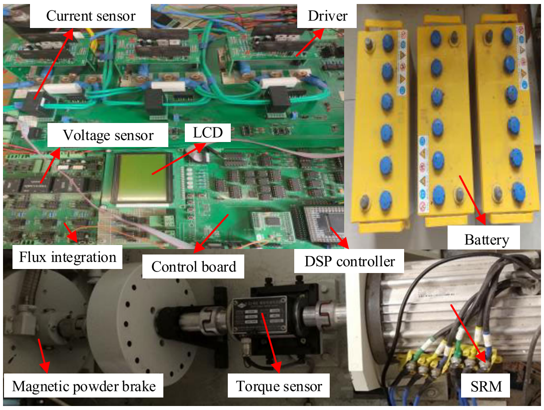

FIGURE 6. Motor control platform.

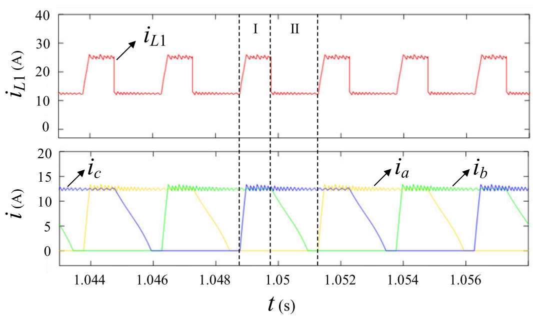

FIGURE 7. Simulation results of three-phase current and sensor *LEM_1*.

is shown in Figure 6 and includes SRM, torque sensor, 36V lead-acid battery, main control board, drive circuit, sampling circuit, asymmetric half-bridge power converter and other related peripheral circuits.

A. SIMULATION

The proposed dual-sensor phase current reconstruction method is simulated and verified, and the control strategy adopts the speed-current dual closed-loop control strategy. The simulation results are shown below.

Figure 7 shows the sampling results of the sensor *LEM*_1 in the low-speed range. The upper and lower channels respectively represent the sampling current of *LEM*_1 and three-phase current. The sampling current of *LEM*_1 can be divided into two intervals in each rotor period as shown in the figure. In interval I, there exist two-phase currents at the same time. The currents of phases A and B are overlapping. In interval II, only one phase current exists, and the other two phases current values are zero. Therefore, the sampling value of *LEM_1* in interval I is twice that of the sampling value in interval II. Since the sensor *LEM_1* is connected in series with the three-phase common excitation and freewheeling circuit, the simulation results are consistent with (4).

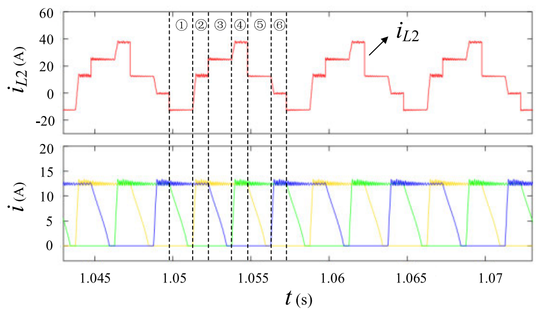

FIGURE 8. Simulation results of three-phase current and sensor *LEM_2*.

Figure 8 shows the simulation results of the sensor *LEM_2* and the three-phase current. Similarly, the sampling current of *LEM_2* are divided into six intervals in one rotor period, corresponding to the above figures ① to ⑥. Take interval ① as an example, in interval ①, phases A and B currents are zero, and only phase C current exists. The corresponding down tubes switching signals *SQ*2, *SQ*4, *SQ*6 are 0, 0 and 1 for each phase, and the sampling value is $-i_c$. In the same way, the analysis results in intervals ② to ⑥ also can be obtained. The waveform in each interval corresponds with the sampling value of the current sensors at different positions in Table 1, indicating that the simulation results are agreement with the theoretical analysis result.

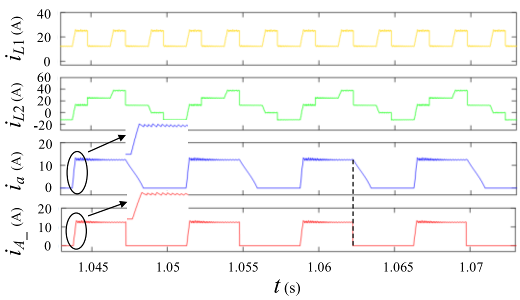

FIGURE 9. Simulation result of reconstruct current.

Figure 9 shows the simulation results of the reconstructed current. Take phase A as an example, the four channels successively represent the sampling results of sensors *LEM*_1 and *LEM*_2, phase A actual and reconstructed current. The partial amplification of the waveform in the ellipses also be shown. As can be seen from the above figure, in the conduction interval of phase A, the reconstructed current waveforms are in good agreement with the actual current. Since the reconstruction method proposed in this paper does not involve demagnetization current, the corresponding phase current will immediately return to zero at the turn-off angle, as shown by the dotted line in the figure above.

B. EXPERIMENTAL VERIFICATION

In order to further verify the correctness of the proposed reconstruction method in this paper, experiments are carried out on the prototype platform shown in Figure 6. The experimental parameters are consistent with the simulation parameters, and the specific experimental results are shown below.

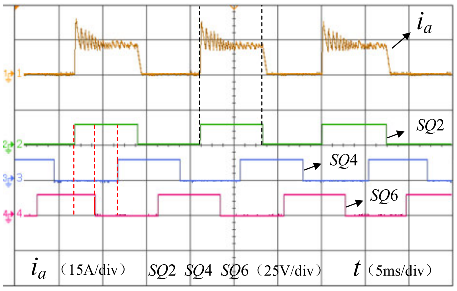

FIGURE 10. Correspondence diagram of actual current and position signal.

Figure 10 shows the three-phase position control signals and the actual current. The turn-on angle is set to 0°, and the turn-off angle is 22.5°. It can be seen from the red dotted line in the above figure that the phase differences of control signals between the two phases are 15°. The black dotted line indicates the turn-on and turn-off angles of phase A.

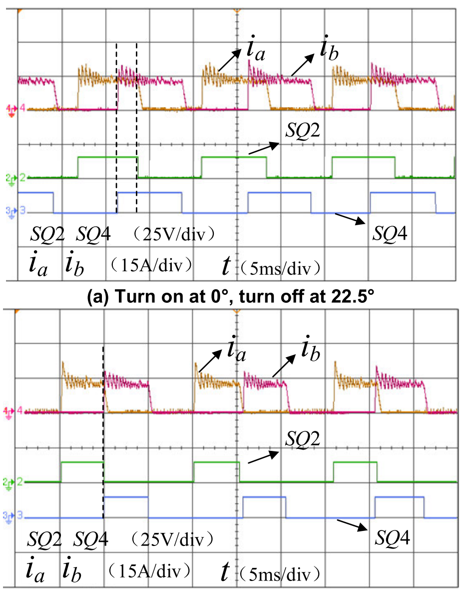

(a) Turn on at 0°, turn off at 22.5°

(b) Turn on at 0°, turn off at 15°

FIGURE 11. Diagram of the relationship between current and position signal at different turn-on and turn-off angles.

Figure 11 shows the current relationship diagrams in different conduction intervals. Also take the phases A and B as an example to illustrate the above experimental results. The turn-on and turn-off angles are also set to 0° and 22.5°. The black dashed line indicates the overlap area of the two phases currents. The conduction interval of each phase and the current overlapping area are large. The current overlapping area between two phases can be shorten By adjusting the turn-on or turn-off angle until the two phases cannot be conducted simultaneously as shown in Figure 11(b). Such as the turn-on angle is 0°, and the turn-off angle is 15°. This result shows two premises of the proposed phase current reconstruction method in this paper: (1) If there is no overlap area, a single sensor can be used to sample the current of each phase without involving any current decoupling process. (2) At most two phases currents exist in the overlapping area at the same time. If there are more than two phases, the number of overlapped phases can be adjusted to two by adjusting the turn-on or turn-off angles. Under this condition, the proposed method also can be used for multi-phase SRM.

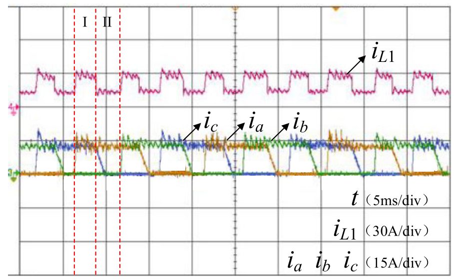

FIGURE 12. Experimental results of three-phase current and sensor *LEM_1*.

Figure 12 shows the waveforms of the three-phase current and the sampling current of *LEM_1*. This result shows that the sampling current of *LEM_1* reaches the maximum when two phases current are overlapped, and its value is the sum of the two-phase currents, which corresponds to the interval I in Figure 8. When only one phase winding has current, the sampling value of *LEM_1* is the smallest, which corresponds to the interval II in Figure 7. The experimental results are the same as the simulation results.

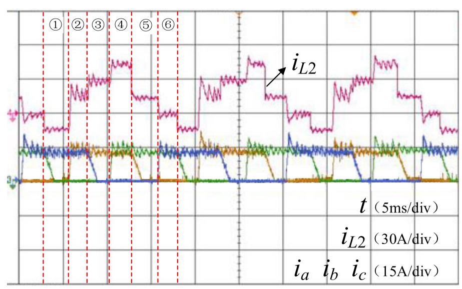

FIGURE 13. Experimental results of three-phase current and sensor *LEM_2*.

Figure 13 shows the waveforms of the three-phase current and the sampling current of *LEM_2*. One rotor period is divided into six internals. Take interval ① as an example,

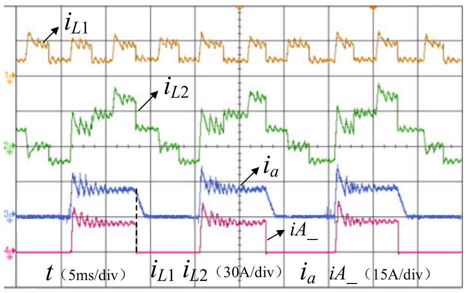

FIGURE 14. Experimental result of reconstruct current.

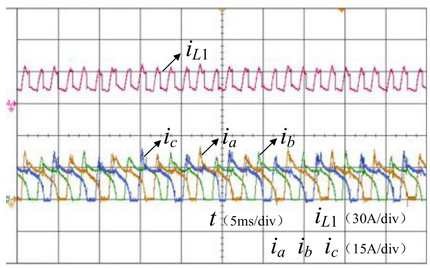

(a) Three-phase current and sensor *LEM*_1 sampling value

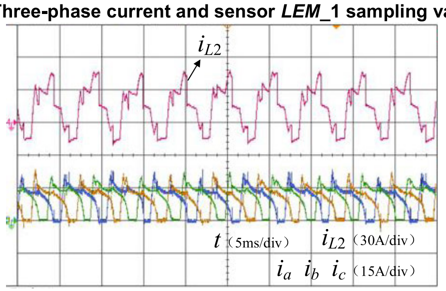

(b) Three-phase current and sensor *LEM*_2 sampling value

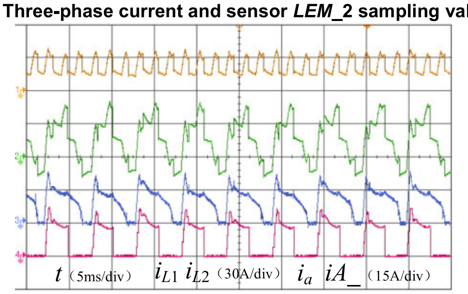

(c) Reconstruction current

FIGURE 15. Experimental results of reconstruction algorithm in high-speed range.

the sampling current in interval ① is $-i_c$, and the phase C is already in the middle of the inductance rising zone, and the overall current ripple is small. The waveform in the intervals ② to ⑥ are the same as the simulation result.

Figure 14 shows the current waveforms of sensors *LEM*_1, *LEM*_2, phase A and its reconstruction in turn. Take phase A as an example, it can be seen from the figure that the actual current and the reconstructed current waveform are approximately the same. The dotted line in the figure also indicates that the reconstruction current immediately returns to zero at the turn-off angle, that is, the reconstruction result does not include the demagnetization current compared with the actual current. The overall reconstruction error is small, and the experimental results are in good agreement with the simulation results.

The above experiments are all carried out with CCC in the low-speed range. In order to further verify the effectiveness of the algorithm in high-speed range, the reconstruction results of the motor in high-speed state also are carried out. Figure 15 shows the experimental results of three-phase current, *LEM*_1, *LEM*_2, and reconstructed current under the high-speed state. It can be seen from the above figure that the sampling currents of the two sensors are not distorted in the high-speed state. Take the phase A as an example in Figure 15(b), the overall waveform and magnitude of the reconstructed current and the actual current are relatively consistent, indicating that the proposed phase current reconstruction algorithm is still feasible in high-speed conditions.

V. CONCLUSION

This paper studies the phase current reconstruction technology of SRMs, and proposes a universal dual-sensor phase current reconstruction method based on the advantages and disadvantages of the existing current reconstruction methods. The theoretical basis, the formula derivation process and the influence of the conduction interval of the proposed method are analyzed and studied in detail. On this basis, the proposed method is extended to multi-phase SRM and the calculation formula of the current reconstruction for each phase is also given. Finally, a three-phase 12/8 structure motor is used to verify the effectiveness of the proposed method by simulation and experiments.

REFERENCES

[1] M. Nassereddine, J. Rizk, and M. Nagrial, "Conversion of a switched reluctance motor to operate as a generator for wind power applications," in *Proc. IEEE Bucharest PowerTech*, Jun. 2009, pp. 1–5.

[2] X. Zhi, D. Xiangjun, and L. Lei, "MPPT for wind power system with switched reluctance generator," in *Proc. 13th IEEE Conf. Ind. Electron. Appl. (ICIEA)*, May 2018, pp. 1420–1424.

[3] A. Ivanov and I. Kalanchin, "Application of maximum power point tracker method in wind energy conversion system based on the switched reluctance generator," in *Proc. Int. Multi-Conf. Eng., Comput. Inf. Sci. (SIBIRCON)*, Sep. 2017, pp. 472–476.

[4] X. Sun, K. Diao, G. Lei, Y. Guo, and J. Zhu, "Study on segmented-rotor switched reluctance motors with different rotor pole numbers for BSG system of hybrid electric vehicles," *IEEE Trans. Veh. Technol.*, vol. 68, no. 6, pp. 5537–5547, Jun. 2019.

[5] S. M. Castano, R. Yang, C. Mak, B. Bilgin, and A. Emadi, "External-rotor switched reluctance motor for direct-drive home appliances," in *Proc. 44th Annu. Conf. IEEE Ind. Electron. Soc. (IECON)*, Oct. 2018, pp. 514–521.

[6] A. Deris Zadeh, E. Adib, H. Farzanehfard, and S. M. Saghaian-Nejad, "New converter for switched reluctance motor drive with wide speed range operation," in *Proc. 2nd Power Electron., Drive Syst. Technol. Conf.*, Feb. 2011, pp. 473–477.

[7] L. Castellini, S. Lucidi, and M. Villani, "Design optimization of switched reluctance motor for aerospace application," in *Proc. IEEE Int. Electric Mach. Drives Conf. (IEMDC)*, May 2015, pp. 1678–1682.

[8] T. L. Skvarenina, O. Wasynczuk, P. C. Krause, W. Z. Chen, R. J. Thibodeaux, and J. Weimer, "Simulation and analysis of a switched reluctance generator/more electric aircraft power system," in *Proc. 31st Intersociety Energy Convers. Eng. Conf.*, Washington, DC, USA, Aug. 1996, pp. 143–147.

[9] Z.-C. You, C.-W. Yu, and S.-M. Yang, "Design of a single-phase DC-excited flux switching machine for home appliance with improved starting toque," in *Proc. Int. Conf. Asian Union Magn. Societies (ICAUMS)*, Aug. 2016, pp. 1–5.

[10] M. Asgar, E. Afjei, A. Behbahani, and A. Siadatan, "A 12/8 double-stator switched reluctance motor for washing machine application," in *Proc. 6th Power Electron., Drive Syst. Technol. Conf. (PEDSTC)*, Feb. 2015, pp. 168–172.

[11] B. Szymanski, H. Kuss, T. Wichert, and K. Kompa, "Switched reluctance motor in textile machine drive," in *Proc. IEEE Power Electron. Spec. Conf.*, Jun. 2008, pp. 2115–2117.

[12] J. Baranowski, T. Drabek, T. Lerch, and P. Piatek, "Case study of switched reluctance motor for use in the electric torque tool," in *Proc. 22nd Int. Conf. Methods Models Autom. Robot. (MMAR)*, Aug. 2017, pp. 1021–1026.

[13] D. Winterborne, M. Shiref, S. Snow, and V. Pickert, "TC48: A low-cost 48 V integrated drive for mild hybrid electric vehicles," *J. Eng.*, vol. 2019, no. 17, pp. 4590–4594, 2019.

[14] Z. Yueying, Y. Chuantian, Y. Yuan, W. Weiyan, and Z. Chengwen, "Design and optimisation of an in-wheel switched reluctance motor for electric vehicles," *IET Intell. Transp. Syst.*, vol. 13, no. 1, pp. 175–182, 2018.

[15] K. Kiyota and A. Chiba, "Design of switched reluctance motor competitive to 60-kW IPMSM in third-generation hybrid electric vehicle," *IEEE Trans. Ind. Appl.*, vol. 48, no. 6, pp. 2303–2309, Nov./Dec. 2012.

[16] M. Takeno, A. Chiba, N. Hoshi, S. Ogasawara, M. Takemoto, and M. A. Rahman, "Test results and torque improvement of the 50-kW switched reluctance motor designed for hybrid electric vehicles," *IEEE Trans. Ind. Appl.*, vol. 48, no. 4, pp. 1327–1334, Jul. 2012.

[17] W. Peng, J. Gyselinck, J.-W. Ahn, and D.-H. Lee, "Optimal current sensor position for switched reluctance motor drives in view of fault detection," in *Proc. IEEE 18th Int. Power Electron. Motion Control Conf. (PEMC)*, Aug. 2018, pp. 852–857.

[18] C. Gan, Q. Sun, J. Wu, C. Shi, and Y. Hu, "A universal two-sensor current detection scheme for current control of multiphase switched reluctance motors with multiphase excitation," *IEEE Trans. Power Electron.*, vol. 34, no. 2, pp. 1526–1539, Feb. 2019.

[19] C. Gan, J. Wu, S. Yang, and Y. Hu, "Phase current reconstruction of switched reluctance motors from DC-link current under double high-frequency pulses injection," *IEEE Trans. Ind. Electron.*, vol. 62, no. 5, pp. 3265–3276, May 2015.

[20] Q. Sun, J. Wu, C. Gan, Y. Hu, N. Jin, and J. Guo, "A new phase current reconstruction scheme for four-phase SRM drives using improved converter topology without voltage penalty," *IEEE Trans. Ind. Electron.*, vol. 65, no. 1, pp. 133–144, Jan. 2018.

[21] Q. Sun, J. Wu, C. Gan, and J. Guo, "A multiplexed current sensors-based phase current detection scheme for multiphase SRMs," *IEEE Trans. Ind. Electron.*, vol. 66, no. 9, pp. 6824–6835, Sep. 2019.

HE CHENG (Member, IEEE) received the B.S. and Ph.D. degrees from the School of Information and Electrical Engineering, China University of Mining and Technology, Xuzhou, China, in 2010 and 2015, respectively. In 2017, he became an Associate Professor with the School of Electrical and Power Engineering, China University of Mining and Technology. His current research interests include electrical motor drives, motor design and control, electric vehicles, and on-board charger for plug-in electric vehicles.

SHUAI MI received the B.S. degree from the China University of Mining and Technology, Xuzhou, China, in 2019, where he is currently pursuing the M.S. degree in electrical engineering. His research interest includes integrated drive system for electric vehicle and permanent magnet synchronous motor.

ZELU WANG received the B.S. degree from the School of Electrical Engineering, Henan University of Technology, Zhengzhou, China, in 2017. He is currently pursuing the M.S. degree in electrical engineering with China University of Mining and Technology, Xuzhou, China. His research interest includes integrated drive system control of electric vehicle switched reluctance motor.

DALI SHAO received the B.S. degree from the School of Electrical and Control Engineering, Xuzhou University of Technology, Xuzhou, China, in 2019. He is currently pursuing the M.S. degree in electrical engineering with China University of Mining and Technology, Xuzhou. His research interest includes integrated drive system for electric vehicle and variable flux reluctance machine.

HAONAN WU received the B.S. degree from the School of Electrical Engineering, Shenyang University of Technology, Shenyang, China, in 2018. He is currently pursuing the M.S. degree in electrical engineering with China University of Mining and Technology, Xuzhou, China. His research interest includes integrated drive system for electric vehicle and permanent magnet synchronous motor.

WENJU YAN (Member, IEEE) received the B.S. and Ph.D. degrees from the School of Information and Electrical Engineering, China University of Mining and Technology, Xuzhou, China, in 2013 and 2018, respectively. Since 2019, he has been a Postdoctoral Researcher with the School of Electrical and Power Engineering, China University of Mining and Technology. His current research interests include switched reluctance motor design, linear launcher, and iron loss analysis.

DONGSHENG YU (Member, IEEE) received the B.Eng. and Ph.D. degrees from the School of Information and Electrical Engineering, China University of Mining and Technology, Xuzhou, China, in 2005 and 2011, respectively. From 2009 to 2010, he was a Visiting Student with The University of Western Australia, Australia. In 2014, he was an Endeavour Research Fellow with The University of Western Australia. He is currently a Full Professor with the School of Electrical and Power Engineering, China University of Mining and Technology. His research interests include power electronics, power line communication, fault monitoring and diagnosis, nonlinear dynamics, and memristive systems. He has published two books and over 60 papers in these areas.